JPE 9-4-14

Design Considerations for a Distributed Generation System Using a Voltage-Controlled Voltage Source Inverter

Sung-Hun Ko*, Su-Won Lee†, Seong-Ryong Lee**, Chemmangot V. Nayar***, and Chung-Yuen Won****

*GAONSolution Incorporated, Kunsan, Korea
†Center for Advanced IT HRD with Close Industry Cooperation, Sungkyunkwan University, Suwon, Korea
** School of Electrical and Information Engineering, Kunsan National University, Kunsan, Korea
***Department of Electrical and Computer Engineering, Curtin University of Technology, Perth, Australia
****Information and Communication Engineering, Sungkyunkwan University, Suwon, Korea

ABSTRACT

Voltage-controlled voltage source inverter (VCVSI) based distributed generation systems (DGS) using renewable energy sources (RES) is becoming increasingly popular as grid support systems in both remote isolated grids as well as end of rural distribution lines. In VCVSI based DGS for load voltage stabilization, the power angle between the VCVSI output voltage and the grid is an important design parameter because it affects not only the power flow and the power factor of the grid but also the capacity of the grid, the sizing of the decoupling inductor and the VCVSI. In this paper, the steady state modeling and analysis in terms of power flow and power demand of the each component in the system at the different values of maximum power angle is presented. System design considerations are examined for various load and grid conditions. Experimental results conducted on a 1 KVA VCVSI based DGS prove the analysis and simulation results.

Keywords: distributed generation system, energy conversion, maximum power angle, VCVSI.

1. Introduction

More than half of the world's population lives in rural areas with unsatisfactory or no access to centralized electricity generation and distribution networks. To complement the poor or no electric situation in these rural areas, the distributed generation system (DGS) using renewable energy source such as PV/diesel hybrid system are becoming increasingly popular. This is because it is one of the most cost-effective, reliable and durable energy sources to provide electricity with good power quality. In a weak gird system, which is characterized by relatively large voltage fluctuation, power outage and surges, the voltage-controlled voltage source inverter (VCVSI) is mostly used as a power line conditioner of the DGS to obtain voltage stabilization[1-8]. The typical configuration of the VCVSI based DGS for weak grids and hybrid micro grids in remote areas are shown Fig. 1. The VCVSI is able to transfer power flow between the DC bus and the AC bus in both directions, either in battery charging mode or

Manuscript received February 5. 2009; revised June 5 2009.
†Corresponding Author: swon@skku.edu
Tel: +82-31-290-7164, Fax: +82-31-299-4164, Sungkyunkwan Univ.
*GAONSolution Incorporated
** School of Electrical & Information Eng., Kunsan National Univ.
***Dept. of Electrical and Computer Eng., Curtin Univ. of Tech.
****School of Information & Communication Eng. Sungkyunkwan Univ.

in inverting mode. The VCVSI is capable of providing load voltage stabilization, reactive power support, demand side management and uninterruptible power supply features [9-15]. The power flow of the system is determined by the power angle between the inverter output and grid voltage and the amplitudes of these voltages [5, 16-18]. When the load voltage is stabilized by a VCVSI in a weak grid, the power angle of the inverter output voltage with respect to the grid is very important since it affects not only power flow and power factor of the grid, but also the required power ratings of each parameter in the DGS.

In this paper, a steady-state model and analysis of a VCVSI based DGS coupled to a weak grid is presented. Design considerations for selecting the appropriate power ratings of the VCVSI and the grid system are included. In order to verify the theoretical model and the design guide, computer simulation supported by experimental results are also presented.

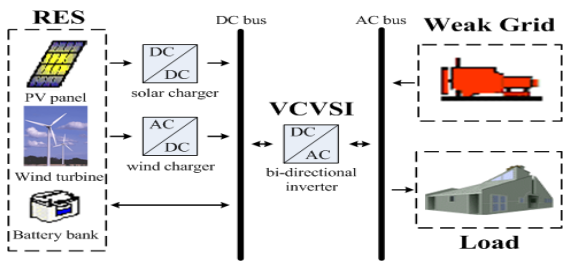

Fig. 1. Typical configuration of the VCVSI based DGS for weak grid.

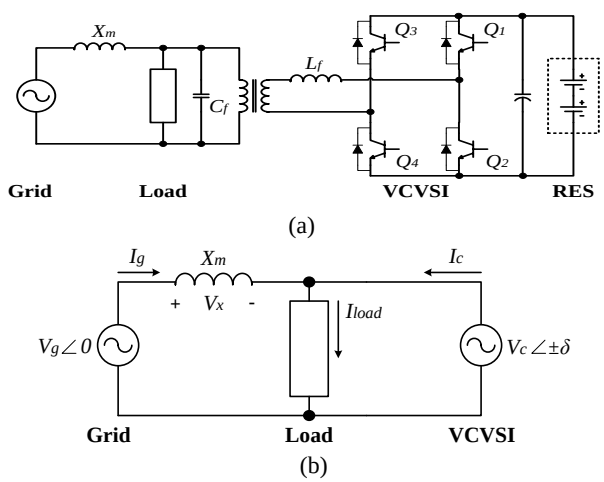

Fig. 2. A topology of the VCVSI based DGS. (a) System topology. (b) The equivalent circuit.

2. Modeling and Analysis of the VCVSI Based DGS

Fig. 2(a) shows a simplified topology of the VCVSI based DGS and Fig. 2(b) shows an equivalent circuit model for the system. The VCVSI is synchronized and connected to the grid through the decoupling inductor (X_m) to prevent huge amount of power flow to or from the grid. This system can transfer active and reactive power between the RES and the AC bus in both directions. The load voltage (V_c) is maintained at a constant by the sinusoidal pulse width modulation of the VCVSI.

From Fig. 2(b), the grid current (I_g) can be expressed as:

$$I_g = \frac{V_g \angle 0 - V_c \angle \delta}{jX_m} = -\frac{V_c \sin\delta}{X_m} - j\frac{V_g - V_c \cos\delta}{X_m} \quad (1)$$

where δ, the power angle, is the phase angle between the inverter voltage (V_c) and the grid voltage (V_g). Assuming that the maximum permitted voltage fluctuation of the weak grid is limited to ±20% and that the load voltage (V_c) can be stabilized at 1.0 per unit (p.u), three possible operational modes can be considered:

- Mode 1: $V_g < V_c$; Minimum V_g = 0.8p.u
- Mode 2: $V_g = V_c$; V_g = 1.0p.u
- Mode 3: $V_g > V_c$; Maximum V_g = 1.2p.u

2.1 Steady-state analysis without load

The phasor diagram of the system without an external load across the VCVSI at the different modes when the grid is responsible for supplying the active power is illustrated in Fig. 3. When the grid voltage changes to V_{g1}, V_{g2} and V_{g3}, the power angle has to be varied in proportion to δ_1, δ_2 and δ_3 respectively to supply the desired power flow. The VCVSI voltage remains constant under this condition i.e. $V_{c1}=V_{c2}=V_{c3}$=1.0p.u. The power angle (δ) could be both lagging or leading, providing either active power flow from the grid to the VCVSI or vice versa. The phase angle (α) between the grid voltage (V_g) and current (I_g) is determined by the magnitude and phase of the voltage across the decoupling inductor (V_x).

Using per unit values ($S_{base}=V^2_{base}/Z_{base}$, $V_{base}=V_c$ and $Z_{base}=X_m$) where V_{base}, Z_{base} and S_{base} are the base voltage,

impedance and apparent power values, respectively, the apparent power of the grid, inverter and the decoupling inductor are given by:

$$S_{gp.u} = P_{gp.u} + jQ_{gp.u} = -V_{gp.u}\sin\delta + j(V_{gp.u}^2 - V_{gp.u}\cos\delta) \quad (2)$$

$$S_{cp.u} = P_{cp.u} + jQ_{cp.u} = -V_{gp.u}\sin\delta + j(V_{gp.u}\cos\delta - 1) \quad (3)$$

$$S_{xp.u} = jQ_{xp.u} = j(V_{gp.u}^2 - 2V_{gp.u}\cos\delta + 1) \quad (4)$$

where $S_{gp.u}$, $S_{cp.u}$ and $S_{xp.u}$ are per unit values of the grid, inverter and decoupling inductor apparent power respectively, and $V_{gp.u}$ is the per unit value of the grid voltage.

Assuming that the output voltage of the VCVSI has to be fixed at 200V(V_c=200V) and S_{base}=1kVA, X_m can be calculated as 40Ω. Proper calculation of X_m based on the power angle and required active power flow through this inductor will be given in section 3.

Using (2) to (4) the theoretical power variation of each parameter in the system for the three possible operational modes can be computed as shown in Fig. 4. The active power varies approximately linear to power angle changes. When the power angle is negative, the active power flows from the grid to the inverter and vice versa, regardless of the grid voltage. However, the reactive power is sensitive to the grid voltage magnitude variations and has nonlinear relationship to the power angle. As can be seen from Fig. 4, the reactive power requirement of the system is supplied by the higher voltage source (V_g or V_c). Thus in Mode 1 (V_g<V_c), the VCVSI supplies the reactive power demanded by the grid (Q_g) and the decoupling inductor (Q_x). In Mode 2 (V_g=V_c), the reactive power required by the decoupling inductor (Q_x) is supplied equally by both the grid and the VCVSI. In Mode 3 (V_g>V_c), Q_x and Q_c is supplied by the grid.

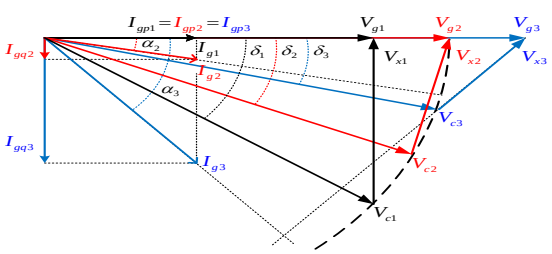

Fig. 3. Phasor diagram of a VCVSI based DGS according to the different modes when no load.

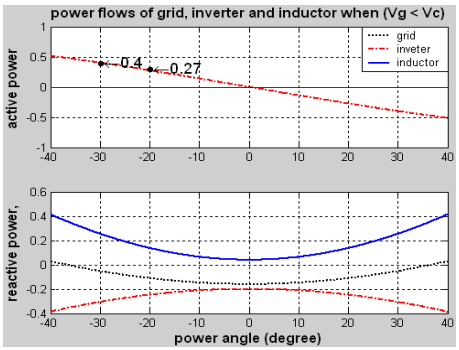

(a)

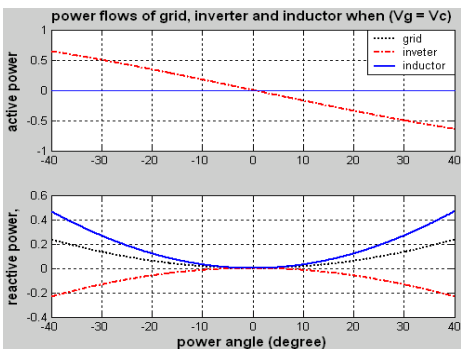

(b)

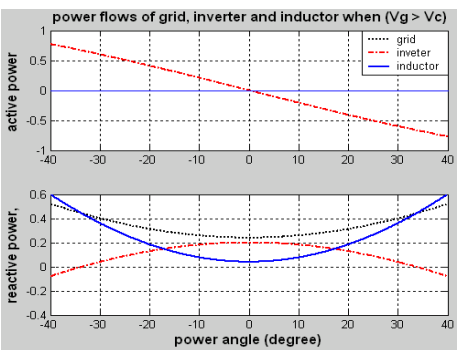

(c)

Fig. 4. Power flow of system versus power angle (δ) at different per unit grid voltages.

Therefore, the reactive power supplied or demanded by the VCVSI can be represented as follows:

$$Q_{cp.u} = \begin{cases} Q_{gp.u} + Q_{xp.u} & when\ V_g < V_c \\ \frac{1}{2}Q_{xp.u} & when\ V_g = V_c \\ Q_{gp.u} - Q_{xp.u} & when\ V_g > V_c \end{cases} \quad (5)$$

where $Q_{gp.u}$, $Q_{cp.u}$ and $Q_{xp.u}$ are per unit values of the grid, inverter and decoupling inductor reactive power, respectively.

Using (2), the variation of the grid power factor at various power angles for the three possible operational modes can be calculated. Fig. 5 illustrates that the power factor of the grid deteriorates when the grid voltage differs from the VCVSI voltage. It is preferable to operate the VCVSI at a higher power angle to improve the power factor of the grid. However, higher power angle results in more reactive power consumption by the decoupling inductor as can be seen in Fig. 4.

2.2 Steady-state analysis with load

Fig. 6 shows the phasor diagram of a system when a reactive load (S_{load}=P_{load}+jQ_{load}) is connected across the VCVSI and the system is operating in Mode 2 (V_g=V_c). Since the load voltage must remain constant to achieve load voltage stabilization, the only controllable parameter in the system is the power angle (δ). From (2) we get:

$$P_g = P_{load} - P_{RES} = -\frac{V_g V_c}{X_m}\sin\delta \tag{6}$$

where, the load active power P_{load} is supplied from the grid and/or from the RES active power P_{RES}.

For demand side management (DSM) operation it is necessary to extract the required power from the RES and supply this power to the load or to the grid. From (6), the power angle (δ) can be expressed as:

$$\delta = \sin^{-1}\left[-\frac{(P_{load} - P_{RES})X_m}{V_g V_c}\right] \tag{7}$$

If the available energy from RES is more than the load demand, then the power angle will be leading to export this extra active power to the grid. In addition, the grid is not required to supply the reactive power of the load as it has to be met by the VCVSI. The VCVSI has to supply the reactive power demand from the load as well as the reactive power demand of the system as given in (5). Hence, (5) can be modified as (8)

$$Q_{cp.u} = \begin{cases} Q_{loadp.u} + Q_{gp.u} + Q_{xp.u} & when\ V_g < V_c \\ Q_{loadp.u} + \frac{1}{2}Q_{xp.u} & when\ V_g = V_c \\ Q_{loadp.u} - (Q_{gp.u} - Q_{xp.u}) & when\ V_g > V_c \end{cases} \tag{8}$$

where, $Q_{loadp.u}$ is per unit value of the load reactive power demand.

Figure 7 shows the block diagram of a VCVSI control system based DGS including the DSM function. In this figure, the Phase Locked Loop (PLL) is responsible for synchronizing the inverter output voltage with the grid voltage. The sampling from the load current, RES voltage (V_{RES}) and current (I_{RES}) is also used to generate the required power angle (δ^*_{ref}) (for DSM operation). Then, after comparing the required/reference values and the actual variables the error signal is generated to feed a PI controller. After generating the desired reference signal, it is given to the PWM generator block[5].

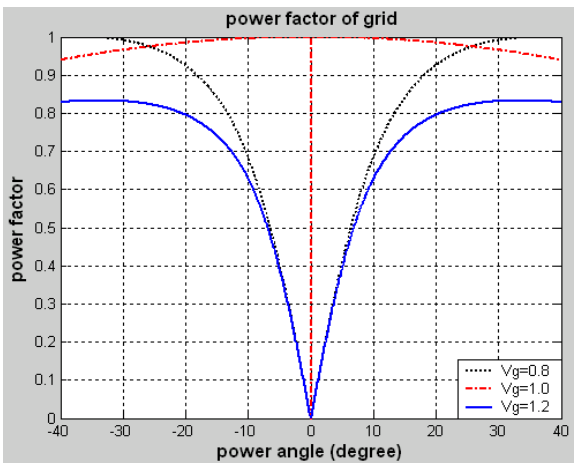

Fig. 5. Power factor versus power angle (δ) in VCVSI based DGS at different per unit grid voltages.

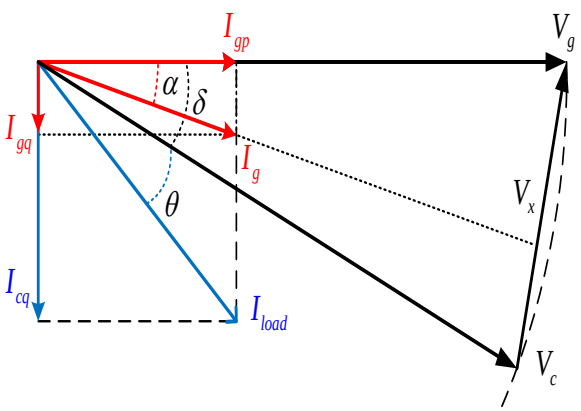

Fig. 6. Phasor diagram of a VCVSI based DGS with the reactive load in Mode 2 (V_g = V_c).

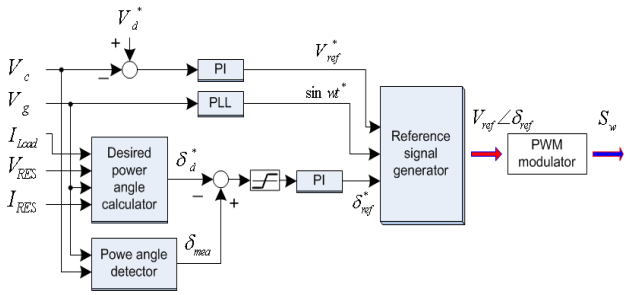

Fig. 7. Control block diagram of the VCVSI-based DGS.

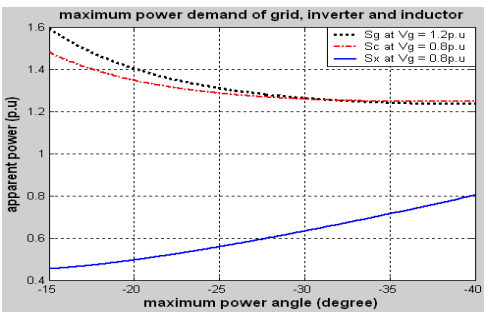

Fig. 8. The maximum power demand of each parameter in DGS according to the maximum power angles for handling the full active power flow.

3. Design Consideration of the System

Based on the discussions in section 2, it is important to specify the maximum power angle (δ_{max}), which will result in optimum sizing of the decoupling inductor, the VCVSI, and the grid. It is a usual practice to limit δ_{max} between 15 to 30 degrees. As can be seen from Fig. 4, if we choose a lower value of δ_{max}, the required power ratings of the grid and the VCVSI will be higher while requiring a smaller decoupling inductor. In a weak grid situation where the capacity of the grid may not be sufficient, the design emphasis must be to use smaller power ratings of the grid and the VCVSI. In this section, the design considerations for choosing a suitable δ_{max}, the required power ratings of the grid, decoupling inductor and the VCVSI are presented. Consider Fig. 4 (Mode 1) where if δ is limited to a maximum of δ_{max}=20°, the active power flow of the system is merely P_g=0.27p.u when the grid voltage is 0.8p.u (V_g<V_c). Therefore, in order to raise the active power flow to P_g=1.0p.u, we need to multiply P_g by a scale factor (D). Using per unit values as mentioned in section 2, this relationship can be expressed as:

$$S_{basep.u} = P_{basep.u} = 1.0\,p.u = D \times P_{gp.u} \tag{9}$$

where, $S_{basep.u}$ and $P_{basep.u}$ is a per unit value of the apparent power (S_{base}) and active power (P_{base}) respectively.

In (9), the scale factor has a maximum value when V_g=0.8p.u. Using (2) and (9), we get:

$$D = 1 \Big/ \left(-0.8 \times \sin \delta_{\max}\right) \tag{10}$$

In order to scale up the active power flow, we need to recalculate $X'_m = X_m / D$. For example, by computing using (10), we get X_m=10.8Ω at δ_{max}=20° and X_m=16Ω at δ_{max}=30°. Thus in order to arrive at the suitable δ_{max}, it is necessary to compute the required maximum power ratings of the grid, X_m and VCVSI in the DGS after considering the proper scale factor in (2) to (4).

Using (5), the maximum power ratings of the grid is when V_g=1.2p.u (Mode 3). However, the power demand of the VCVSI has a maximum value when V_g=0.8 (Mode 1). The required maximum apparent power of the grid (S_g), decoupling inductor (S_x), and the VCVSI (S_c) at different δ_{max} is shown in Fig. 8. It can be seen that S_x is proportional to δ_{max} while S_g and S_c decreases as δ_{max} increases. In a weak grid system, improving the grid power factor and reducing S_g and S_c are more important than the reactive power S_x across the inductor. Considering these factors and referring to Fig. 5 and 8, a maximum power angle of 30° is more suitable.

In addition, we also need to consider the effect of the system load on S_g, S_x, and S_c by using (6) to (8). This is presented in Fig. 9 to 11. Fig. 9 and 10 show the variation of the apparent power demand of the grid and inductor as the load is varied from no load to full load. It may be noted that Q_g and Q_x are not affected by the reactive component of the load and therefore for computation purpose only a purely resistive load variation is considered. Fig. 9 shows that S_g at δ_{max}=30° is smaller than δ_{max}=20° with V_g=1.2p.u (Mode 3). This means that the grid capacity can be downsized from 1.41p.u at 20° to 1.26p.u at 30° when delivering a full load. However, as shown in Fig. 10, S_x is 0.64p.u at δ_{max}=30° compared to 0.5p.u at δ_{max}=20° in the full load condition. In this simulation, we

choose V_g=0.8p.u (Mode 1) because the operating power angle is maximum.

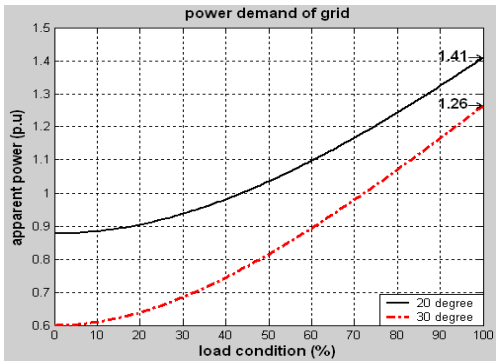

Fig. 9. The required power ratings of grid from no load to full resistive load at the maximum power angle (20° and 30°).

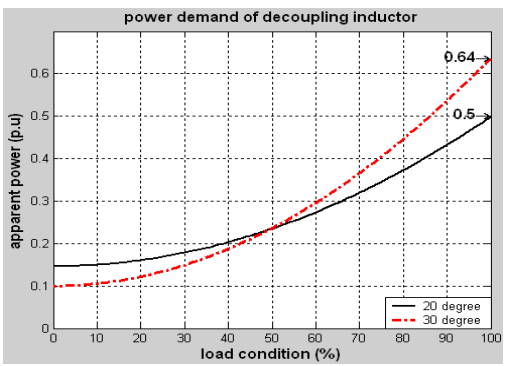

Fig. 10. The required power ratings of decoupling inductor from no load to full resistive load at the maximum power angle (20° and 30°).

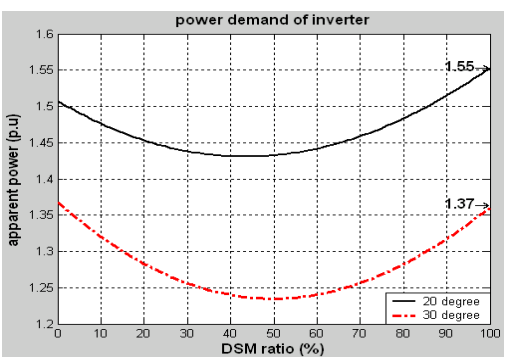

Fig. 11. The required power rating of VCVSI corresponding to DSM ratio when the full load with a load angle of 36.9° (Z=1p.u∠36.9°).

Fig. 11 shows the required power rating of the VCVSI at δ_{max}=20° and 30° when the load is rated 1.0p.u at the load angle of 36.9° and various DSM values. The VCVSI capacity (S_c) should be considered when the load is reactive because the VCVSI is responsible for supplying the required apparent power ratings of the DGS as well as the reactive power of the load. In addition, the VCVSI has to supply a portion of the active power of the load besides meeting the reactive power demand in the DSM operating mode. Assuming a general purpose load (load power factor angle of 36.9° for the full load demand), S_c rating is calculated based on the DSM ratio (which is the ratio of the active power supplied by the RES to the rating of the load). Fig. 11 shows that the VCVSI capacity can be downsized from 1.55p.u at 20° to 1.37p.u at 30° when the DSM ratio is 100%. For system design, it is recommended that the apparent power rating of the grid, decoupling inductor and the VCVSI when supplying a load of 1.0p.u, is greater than 1.26p.u, 0.64p.u, and 1.37p.u respectively.

4. Experimental Results

Experiments were conducted on a 1 KVA VCVSI based DGS to verify the analysis and simulation results. The parameters used in the experimental system and specifications are given in Table 1 and 2. A photograph of the experimental set up is shown in Fig. 12.

Table 1. Experimental parameters

Parameters		Values	Parameters	Values
V_{AC}		200±40 V	V_{DC}	200V
Full load		1KVA	Transformer Turn ratio	1:2
Frequency		60Hz	Fsw	10KHz
L_m	20°	29mH	L_f	0.3mH
	30°	42.4mH	C_f	6.88uF

• where L_m is decoupling inductor, L_f is the filter inductor and C_f is the filter capacitor.

The Voltech (PM3000A) power meter was used to measure a power ratings and power factor. The Tektronix

(TDS3054B) digital scope was used to capture the following results.

Table 2. System specifications

Specification	Part Number	Manufacturer
IGBT	2MB75L060	FUJI
Battery	ITX40	ATLASBS
DSP	TMS302C33	TI
Voltage sensor	LV25P	LEM
Current sensor	LA25P	LEM
Protection and dead time circuit	XC95144XL	XILLINGS

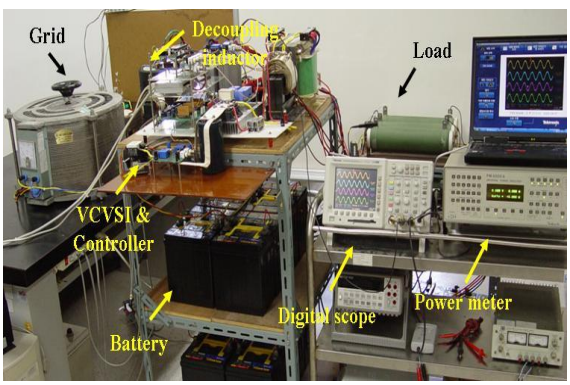

Fig. 12. A photograph of the proposed VCVSI based DGS.

Fig. 13 shows the waveforms of the system when supplying the full resistive load of 1.0p.u (R=40Ω) at V_g= 0.8p.u (160[V]). The voltage and current waveforms of the grid and load at δ_{max}=20° are shown in Fig. 13(a) and δ_{max}=30° in Fig. 13(b). The load voltage and current are 200[V] and 5[A], and power factors at δ_{max}=20° and 30° are measured as 0.897 and 0.96 respectively. This means that the system can provide load voltage stabilization while supplying active power from the grid. Fig. 14 shows the experimental waveform results of DSM ratio of 50[%] supplied by VCVSI in DGS with a 100% resistive load at V_g=1.0p.u. The grid current is reduced to half the load current; the other half is supplied by the VCVSI.

Fig. 15 shows the grid voltage, load voltage and grid current waveform when the grid voltage is changed from 1.0p.u (200V) to 0.8p.u (160V). The load voltage is maintained at 1.0p.u without being affected by the grid voltage fluctuations.

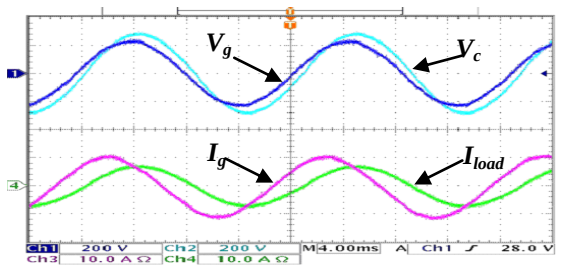

(a) δ_{max} =20 °

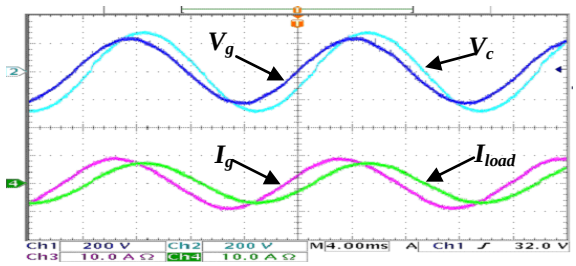

(b) δ_{max} =30°

Fig. 13. Experimental waveforms of system at each maximum power angle. (Y-axis: V_g=200[V/Div.], V_c=200[V/Div.], I_g=10[A/Div.], I_c=10[A/Div.], X-axis: 4[ms/Div.]).

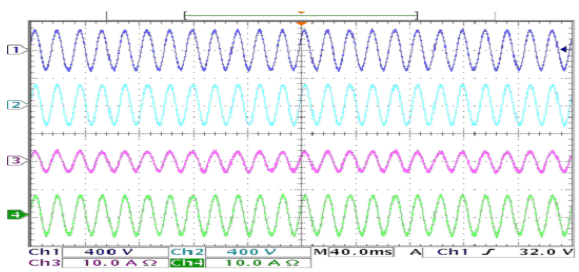

Fig. 14. Experimental waveforms of DSM operation in DGS. Ch1:Grid voltage(V_g), Ch2:Inverter voltage(V_c), Ch3:Grid current(I_g), Ch4:Load current(I_c). (Y-axis: V_g=400[V/Div.], V_c=400[V/Div.], I_g=10[A/Div.], I_c=10[A/Div.], X-axis: 40[ms/Div.]).

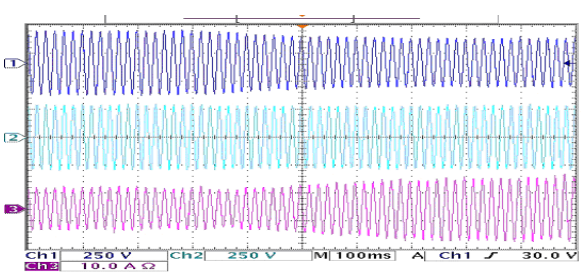

Fig. 15. Experimental waveform results of the voltage stabilization in the system. Ch1:Grid voltage(V_g), Ch2: Inverter voltage(V_c), Ch3: Grid current(I_g). (Y-axis: V_g=250[V/Div.], V_c=250[V/Div.], I_g=10[A/Div.], X-axis: 100[ms/Div.]).

The apparent power of the grid, decoupling inductor and the VCVSI in the DGS are measured as shown in Fig. 16, 17 and 18 respectively. These experiments were performed at the same condition as the simulation shown previously in Fig. 9, 10 and 11. As can be seen in Fig. 16 to 18, the experimental results at δ_{max} = 20° and 30° according to various operating conditions in DGS are similar to the simulation results. From these experimental results and the simulation results (Fig. 9 to 11), the required maximum power rating of the grid, decoupling inductor, and the VCVSI are summarized in Table 3.

The variation of the grid power factor when the load is varied from zero to full resistive load corresponding to δ_{max}= 20° and 30° for the three possible operational modes is presented in Fig. 19.

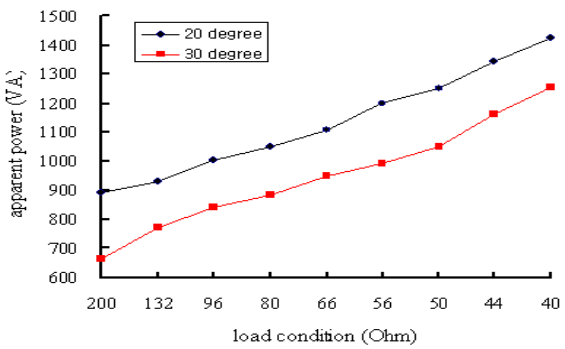

Fig. 16. Experimental results of apparent power ratings of grid from no load to full resistive load at the maximum power angle. (20° and 30°)

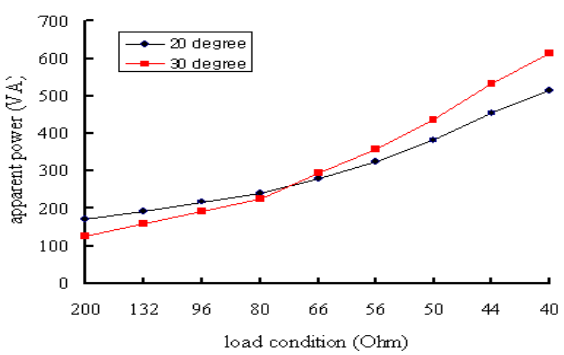

Fig. 17. Experimental results of apparent power ratings of decoupling inductor from no load to full resistive load at the maximum power angle. (20° and 30°)

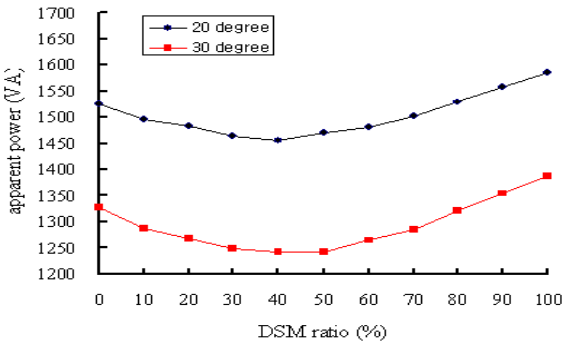

Fig. 18. Experimental results of apparent power ratings of VCVSI corresponding to DSM ratio when the full load with phase angle of 36.9° .(Z=1.0p.u∠36.9°)

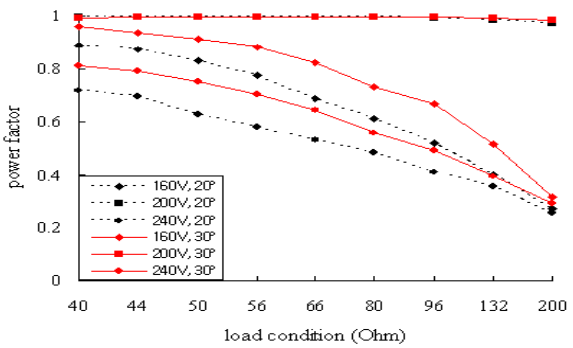

Fig. 19. Experimental results of power factor of grid from no load to full resistive load at each maximum power angle and the three possible operational modes.

From this (Fig. 19), it can be concluded that the VCVSI based DGS should be operated at the higher δ_{max} to obtain a better grid power factor. Using the larger maximum power angle has the additional benefit of obtaining higher resolution when the system controller is implemented using a digital signal processor. For example, the resolution of the controllable active power of the system at the maximum power angle of 30° is 3.3% of the required power ratings per degree compared to that of 5% per degree at 20°.

The design considerations and the comparison of the VCVSI based DGS at various δ_{max} can be summarized as follows:

1) The suitable maximum power angle of the VCVSI based DGS is 30°.

Table 3. The required maximum power rating of the grid, decoupling inductor and the VCVSI.

Components	Conditions				Power rating (VA)	
	Mode	Load	DSM ratio (%)	δ_{max}	Simulation	Experiment
Grid (S_g)	III (240V)	Full (40Ω)	0	20°	1410	1424
				30°	1260	1257
Inductor (S_x)	I (160V)	Full (40Ω)	0	20°	500	514
				30°	640	616
VCVSI (S_c)	I (160V)	Full (40Ω∠36.9°)	100	20°	1550	1586
				30°	1370	1388

2) The power capacity demand of the grid, decoupling inductor and VCVSI with respect to a load of 1.0p.u has to be considered greater than 1.3p.u, 0.62p.u and 1.4p.u respectively.

5. Conclusions

This paper presents the steady–state performance analysis and design consideration of a grid-interactive VCVSI based DGS for weak grid application. The power flow and the required power ratings of each parameter in the DGS according to the limitation of the power angle range are presented and a suitable maximum power angle for this system is suggested. Design considerations of the VCVSI based DGS are verified by conducting experiments on a 1KVA prototype for various load conditions. The experimental results verify the design consideration, theoretical analysis and computer simulations. This result could be useful as a design guide line for the VCVSI based DGS.

Acknowledgment

This work was supported in part by the New & Renewable Energy Development project (2007-N-PV08-03 -0) of the KEMCO.

References

[1] W. Wongsaichua, W. J. Lee, S. Oraintara, C. Kwan, and F. Zhang, "Integrated high-speed intelligent utility tie unit for disbursed/renewable generation facilities," *IEEE Trans. Ind. Appl.*, Vol. 41, Nno. 2, pp. 507- 513, 2005.

[2] T. Jin, L. Li, and K. Smedley, "A universal vector controller for three-phase PFC, APF, STATCOM, and grid-connected inverter," *in Proc. of APEC'04*, pp. 594-600, 2004.

[3] F. Blaabjerg, Z. Chen, and S.B. Kjaer, "Power electronics as efficient interface in dispersed power generation systems," *IEEE Trans. Power Electron.*, Vol. 19, No. 5, pp. 1184 - 1194, 2004.

[4] M. Dai, M.N. Marwali, J. W. Jung, and A. Keyhani, "Power flow control of a single distributed generation unit with nonlinear local load," *in Proc. of PES*, pp. 398-403, 2004.

[5] S.H. Ko, S.R. Lee, H. Dehbonei, and C.V. Nayar, "Application of Voltage and Current Controlled Voltage Source Inverters for Distributed Generation Systems," *IEEE. Trans. Energy Convers.*, Vol. 21, No. 3, pp. 782-792, 2006.

[6] C.V. Nayar, "Control and interfacing of bi-directional inverters for off-grid and weak grid photovoltaic power systems," *in Proc. of PES Summer Meeting*, pp. 1280-1282, 2000.

[7] H. Dehbonei, C.V. Nayar, L. Borle, "A Combined Voltage Controlled and Current Controlled 'Dual Converter' for a Weak Grid Connected Photovoltaic System with Battery Energy Storage," *in Proc. of PESC'02*, pp. 1495-1500, 2002.

[8] M. Prodanovic, and T.C. Green, "Control and filter design of three-phase inverters for high power quality grid connection," *IEEE Trans. Power Electron.*, Vol. 18, No. 1, pp. 373 - 380, 2003.

[9] K. Dai, P. Liu, J. Xiong and J. Chen, "Study on dual-DSP-controlled three-phase series-parallel compensated line-interactive UPS system (delta- conversion UPS)," *in Proc. of IEMDC'03*, pp. 436-442, 2003.

[10] A. Baronian, and S. Dewan, "An Adaptive Digital Control of Current Source Inverter Suitable for Parallel Processing Inverter Systems," *in Proc. of IEEE 30th Ann. Meeting, Industry Applications Conf.*, pp. 2670-2677, 1995.

[11] H. Dehbonei, "Power Conditioning for Distributed

Renewable Energy Generation," Ph.D. Dissertation, Dept. elect. Comput. Eng., Curtin Univ. Technol., perth, 2003.

[12] M.N. Marwali, and A. Keyhani, "Control of distributed generation systems-Part I: Voltages and currents control," *IEEE Trans. Power Electron*., Vol. 19, No. 6, pp. 1541-1550, 2004.

[13] T.Kawabata, K. Ogasawara, N. Sashida, Y. Yamamoto, and Y. Yamasaki, "Parallel processing inverter system," *IEEE Trans. Power Electron.*, Vol. 6, No. 3, pp. 442-450, 1991.

[14] Z. Chen, and E. Spooner, "Voltage source inverters for high-power, variable-voltage DC power sources," *Inst. Elect. Eng-Proc. Gen., Transm. Distrib.*, Vol. 148, No. 5, pp. 439-447, 2001.

[15] L. Borle, M. S. Dymond, and C.V. Nayar, "Development and Testing of a 20-KW Grid Interactive Photovoltaic Power Conditioning System in Western Australia," *IEEE Trans. Ind. Appl.*, Vol. 33, No. 2, pp. 502-508, 1997.

[16] M. Ashari, W. W. L. Keerthipala, and C.V. Nayar, "A Single Phase Parallel Connected Uninterruptible Power Supply/Demand Side Management System," *IEEE Trans. Energy Convers.*, Vol. 15, No. 1, pp. 97 - 102, 2000.

[17] M. Ashari, C.V. Nayar, and S. Islam, "Steady-state performance of a grid interactive voltage source inverter," *in Proc. of PES Summer Meeting*, pp. 650-655, 2001.

[18] H. Dehbonei, C. V. Nayar, and L. Borle, "A multifunctional power processing unit for an off-grid PV diesel hybrid power system," *in Proc. of PESC'04*, pp. 1969-1975, 2004.

Sung-Hun Ko received his B.Sc. and M.S.c degrees in the Department of Control and Instrumentation Engineering from the Kunsan National University, Kunsan, Korea in 1998 and 2000, respectively, and his Ph.D. degree from Kunsan National University, Kunsan, Korea, in 2007. From 2004 to 2005, he was the Visiting Research Fellow with the Department of Electrical and Computer Engineering at Curtin University of Technology, Perth, Australia. From 2007 to 2008, he was the Postdoctoral with the Chonbuk National University, Jeonju, Korea. Currently, he is working as a technology director with the GAONSolution, Inc., Korea. His current research interests include soft-switching inverter, power factor correction, inverter control and renewable energy based distributed generation system.

Su-Won Lee received his B.Sc., M.Sc., and Ph.D. degrees in Electrical Engineering from Chonbuk National University, Jeonju, Korea in 1991, 1993, and 1998, respectively. He was a Research Professor with BK21 Kunsan National University from 2001 to 2006. He was a Research Professor with Institute of TMS Information Technology at Yonsei University from 2006 to 2008. Currently, he is a research professor with the Center for Advanced IT HRD with Close Industry Cooperation at Sungkyunkwan University. His research interests include bi-directional dc/dc converter, inverter control and renewable energy based distributed generation system

Seong-Ryong Lee received his B.Sc. and M.S.c degrees in Electrical Engineering from Myong-Ji University, Seoul, Korea in 1980 and 1982, respectively, and his Ph.D. degree from Chonbuk National University, Jeonju, Korea, in 1988. From 1997 to 1998, he was the Visiting Professor with the Department of Electrical and Computer Engineering at Virginia Tech, USA. From 2002 to 2004, he was the Director of Engineering Research Institute at Kunsan National University, Kunsan, Korea. From 2004 to 2006 he was the Visiting Professor with the Department of Electrical and Computer Engineering at Curtin University of Technology, Perth, Australia. Since 1990, he is a professor with the Dept. of Control, Robot, and System Engineering at Kunsan National University. Currently, he is working as a Dean of College of Engineering at Kunsan National University. His current research interests include soft-switching inverter, power factor correction, switch mode power supply, and renewable energy based distributed generation system.

Chemmangot V. Nayar received his B. Tech. degree in Electrical Engineering from the University of Kerala, India, in 1969, his M. Tech. degree in Electronics from the Indian Institute of Technology, Kanpur, in 1976, and his Ph.D. degree in Electrical Engineering, specializing in wind electrical power generation, from the University of Western Australia, Perth, Australia, in 1985. He holds a Personal Chair in Electrical Engineering at Curtin University of Technology. Prof. Nayar is a Chartered Engineer and Corporate Member of IEE, and a Chartered Professional Engineer and Fellow of IEAust.

Chung-Yuen Won was born in Korea in 1955. He received his B.S degree in Electrical Engineering from Sungkyunkwan University, Suwon, Korea, in 1978, and his M.S. and Ph.D. degrees in Electrical Engineering from Seoul National University, Seoul, Korea, in 1980 and 1988, respectively. From 1990 to 1991, he was with the Department of Electrical Engineering, University of Tennessee, Knoxville, as a Visiting Professor. Since 1988, he has been with the faculty of Sungkyunkwan University, where he is currently a Professor in the School of Information and Communication Engineering; he is also a dean in the department of photovoltaic system engineering. His research interests include dc-dc converters for fuel cells, electro-magnetic modeling and prediction for motor drives, and control systems for rail power delivery applications.